



HAL
open science

La_{1.5}Nd_{0.3}Pr_{0.2}NiO_{4.16}: A new cathode material for IT-Solid Oxide Fuel Cells

Sabah Amira, Mosbah Ferkhi, Fabrice Mauvy, Sébastien Fourcade,
Jean-Marc. Bassat, Jean-Claude Grenier

► **To cite this version:**

Sabah Amira, Mosbah Ferkhi, Fabrice Mauvy, Sébastien Fourcade, Jean-Marc. Bassat, et al..
La_{1.5}Nd_{0.3}Pr_{0.2}NiO_{4.16}: A new cathode material for IT-Solid Oxide Fuel Cells. *Electrocatalysis*,
2023, 14 (4), pp.546-560. 10.1007/s12678-023-00818-x . hal-04027196

HAL Id: hal-04027196

<https://hal.science/hal-04027196>

Submitted on 13 Mar 2023

HAL is a multi-disciplinary open access archive for the deposit and dissemination of scientific research documents, whether they are published or not. The documents may come from teaching and research institutions in France or abroad, or from public or private research centers.

L'archive ouverte pluridisciplinaire **HAL**, est destinée au dépôt et à la diffusion de documents scientifiques de niveau recherche, publiés ou non, émanant des établissements d'enseignement et de recherche français ou étrangers, des laboratoires publics ou privés.

La_{1.5}Nd_{0.3}Pr_{0.2}NiO_{4.16} : a New Cathode Material for IT-Solid Oxide Fuel Cells

S. Amira^{1,2}, M. Ferkhi^{1,2,3*}, F. Mauvy³, S. Fourcade³, J.M. Bassat³, J.C. Grenier³

¹ *Département de Chimie, Faculté des Sciences Exactes et Informatique, Université Mohamed Seddik Ben Yahia, BP98 Ouled Aissa, 18000 Jijel, Algeria.*

² *Laboratoire d'Etude sur les Interactions Matériaux-Environnement (LIME), Université Mohamed Seddik Ben Yahia, BP98 Ouled Aissa, 18000 Jijel, Algeria.*

³ *CNRS, Univ. Bordeaux, Bordeaux INP, ICMCB, UMR 5026, F-33600 PESSAC Cedex, France*

Abstract

The La_{1.5}Nd_{0.3}Pr_{0.2}NiO_{4.16} material was prepared by the citrate method and used as a cathode for Solid Oxide Fuel Cell (SOFC). The study was carried out in the presence of a thin interfacial layer composed of 50% GDC10 and 50% 8YSZ deposited on both surfaces of the GDC10 (Ce_{1.9}Gd_{0.1}O_{1.95}) electrolyte. The purity of the materials was studied by X-ray diffraction, while X-ray Photon-electron Spectrometry (XPS) was used to characterize the surface chemical state of the synthesized material; the morphology of the electrode and cross-sectional images of the cell were obtained by Scanning Electron Microscopy (SEM). Iodometric titration has also been performed for evaluating oxygen over-stoichiometry. Cross-section SEM images have shown good adherence between all the cell components and the cationic character of the cathode material was confirmed by the XPS and Iodometric analysis. The use of these materials as an oxygen cathode has shown interesting electrochemical properties with an Area Specific Resistance (ASR) value of the order of 0.060 (Ω.cm²) at 600 °C and 0.022 (Ω.cm²) at 700 °C. The activation energy (E_a) of the LNPNO5 material is very low and is of the order of 0.96 eV.

Keywords: Solid oxide fuel cell, New cathode materials, New interface layer, Electrochemical impedance spectroscopy, Area specific resistance.

I. Introduction

SOFCs are the most promising fuel cells insofar as their high-temperature operation allows cogeneration. The efficiency of the assemblies reaches 60 and 70 % if the gases are pressurized at the inlet of the cell. Their power can range from 10 Kilowatts to a few Megawatts [1]. Despite the efforts made in this area, the operation temperature of SOFCs remains still a challenge. The reduction in temperature towards intermediate temperature causes an increase in the ohmic drop in the electrolyte and leads to the creation of over-voltages at the electrodes, mainly at the oxygen electrode. Current research is directed toward the discovery of new cathode, electrolyte, and anode materials having good electrochemical properties to overcome the problems encountered during the operation of electrochemical cells [2-5].

Among these studies, the use of an interfacial layer between the electrolyte and cathode has been shown to be efficient for preventing chemical reactivity and significantly increasing the mechanical and electrochemical properties of the cathode [6-11]. The addition of a "diffusion barrier" layer to the interface blocks the diffusion of cationic species at the interface preventing, subsequently, the formation of insulating secondary phases. It has also been shown that poor adhesion between cathode materials and electrolytes can lead to larger interface bias resistance due to a bad contact area. The interlayer improves the adhesion between the cathode and the electrolyte, preventing the decrease of the electrode performance during cell operation. The majority of studies carried out on the interface layers have focused mainly on ceria, CeO_2 , substituted for samarium [12], gadolinium [13], or yttrium [14]. T. Ogier *et al.* [8] found that the presence of a layer of $\text{Ce}_{0.8}\text{Gd}_{0.2}\text{O}_{2-\delta}$ (GDC) or $\text{Ce}_{0.72}\text{Y}_{0.18}\text{O}_{2-\delta}$ (YDC) between the cathode materials $\text{La}_{0.6}\text{Sr}_{0.4}\text{Fe}_{0.8}\text{Co}_{0.2}\text{O}_{3-\delta}$, $\text{La}_2\text{NiO}_{4+\delta}$, $\text{Pr}_2\text{NiO}_{4+\delta}$ or $\text{Nd}_2\text{NiO}_{4+\delta}$ and the 8YSZ electrolyte significantly reduced the polarization resistances due to an improvement in the contact surface between the cathode and the electrolyte. Steele *et al.* [9] showed that a layer of $1\mu\text{m}$ of $\text{La}_{0.6}\text{Sr}_{0.4}\text{Co}_{0.2}\text{Fe}_{0.8}\text{O}_{3-x}$ (LSCF) adjacent to the gadolinium-doped cerium oxide reduced the value of the ASR by a factor of 2 to 3.

Through easy spin-coating, Jang *et al.* [15] recently described a structure for a newly designed interfacial layer consisting of a GDC barrier layer and a thin LSCF layer. This study showed that a high surface area of the nano-web-structured $\text{La}_{0.6}\text{Sr}_{0.4}\text{Co}_{0.2}\text{Fe}_{0.8}\text{O}_{3-\delta}$ (NW-LSCF) was obtained and the ORR was improved due to an increased three-phase limiting length.

On the other hand, some studies have tended to use composite materials. The latter makes it possible to delocalize the surface of contact of two dimensions towards a contact in three dimensions (i.e. in volume). This depends on the known properties of electrolyte materials YSZ,

GDC, and SDC ($\text{Ce}_{0.8}\text{Sm}_{0.2}\text{O}_{1.90}$) which were previously studied and used in SOFC. For this purpose, Raghvendra et al. [16], by studying and developing composite materials consisting of YSZ and SDC, concluded that increasing the weight ratio of SDC increases the electrical conductivity. For a weight ratio of 8.5:1.5 (YSZ/SDC), the electrical conductivity was found to be larger than that of YSZ in the temperature range of 400–700 °C. Electrode polarisation was also significantly reduced with SDC in the composite electrolytic system. The 1:1 size ratio of dense yttria-doped ceria (YDC) and yttria-stabilized zirconia (YSZ) nanocomposites [17], also showed significant improvement in total ion conductivity with a decrease in crystallite size, attributed to an almost ideal parallel connection between the two nanophases, coupled with an increase in their ion diffusivity at the grain boundaries.

Moreover, the presence of the YSZ phase has been shown to considerably improve the mechanical properties of the cell.

On the cathode side, two types of materials have been used; at first, electronic conductors mixed with the electrolyte to make a composite electrode, and later on, Mixed Electronic and Ionic Conducting oxides (MIEC) [2-5, 18]. It is a means of delocalizing the oxygen reduction reaction within the whole volume of the electrode (reduction at the surface of the grains) [19], and of reducing the associated polarization resistances and over-voltages [20]. Typical cathode materials are compounds with a perovskite structure, as for instance, the widely studied strontium cobaltites $\text{La}_{1-x}\text{Sr}_x\text{CoO}_{3-\delta}$ (LSCO) and strontium lanthanum Ferro-cobaltites $\text{La}_{1-x}\text{Sr}_x\text{Co}_{1-y}\text{Fe}_y\text{O}_{3-\delta}$ (LSCF) [21].

During the last fifteen years, the A_2BO_4 materials (Ruddlesden-Popper phases) have been widely studied as SOFCs cathodes and have drawn a lot of attention due to their kinetics of oxygen surface exchange and their oxygen diffusion which are higher than those of the ABO_3 oxides [22]. Actually, and contrarily to perovskite-type materials which are oxygen deficient, A_2BO_4 oxides can accommodate excess oxygen (δ) as an interstitial oxygen defect. This oxygen over-stoichiometry δ ($\text{A}_2\text{BO}_{4+\delta}$) leads to high oxygen mobility in these two-dimensional structures starting already at intermediate temperatures (around 500 °C) [23]. In addition, in these oxides, the presence of interstitial oxygen atoms simultaneously induces the mixed valence of the transition metal, $\text{B}^{2+} / \text{B}^{3+}$, which results in high electronic conductivity [24].

A lot of work focused on the electrochemistry and transport properties of $\text{Ln}_2\text{NiO}_{4+\delta}$ phases, where Ln = La, Pr or Nd, with particular attention to the $\text{La}_2\text{NiO}_{4+\delta}$ composition. Skinner *et al.* [23] and Bassat *et al.* [24] have studied unsubstituted materials and found high oxide ionic conductivities over a wide temperature range indicating that the nickelates are promising cathode materials for SOFC cells.

It was discovered in a previous work by Ferkhi *et al.* [5] that the synthesis of the lanthanum nickelate materials doped with two rare earth elements is possible and leads to very interesting electrochemical properties at low temperatures when used as a cathode for the ORR process in alkaline media. In this study, it was concluded that $\text{La}_{1.5}\text{Nd}_{0.3}\text{Pr}_{0.2}\text{NiO}_{4.16}$ (LNPNO5) compound leads to a current intensity very close to the platinum electrode one, which allows them to be used as a bifunctional electrocatalyst for the reduction of oxygen in alkaline media.

In this paper, we aim to investigate the possible efficiency of the association of this nickelate composition with an innovative thin interfacial layer, to our knowledge, *i.e.* a mixture made of GDC and YSZ (so-called GDC-YSZ). According to the results reported by Montenegro-Hernandez [25], for instance, it is well known that, when deposited on YSZ, such materials with high La content lead to the formation of insulating $\text{La}_2\text{Zr}_2\text{O}_7$ and La_2O_3 phases. When using the GDC-YSZ mixture as an interfacial layer, we hope to increase the adherence between GDC and the nickelate which is less detrimental while keeping quite high sintering temperatures. Moreover, our second goal was to improve the thermomechanical adhesion between the three layers, *i.e.* GDC, the interfacial layer, and the cathode in order to decrease the contact resistances. This is finally why our cathode composition contains a limited amount of La, in order to prevent the chemical reactivity as already explained.

In light of all the data summarized here above, a new cathode material based on $\text{La}_{1.5}\text{Nd}_{0.3}\text{Pr}_{0.2}\text{NiO}_{4+\delta}$ (LNPNO5) was developed and was deposited symmetrically on a GDC10 ($\text{Ce}_{1.9}\text{Gd}_{0.1}\text{O}_{1.95}$) pellet on which an interlayer composed of 50% 8YSZ and 50% GDC10 (GDC-YSZ) has been, beforehand, deposited on both sides of the GDC10. The symmetrical cell obtained at the end is schematized as follows: LNPNO5 /GDC-YSZ/GDC/ GDC-YSZ /LNPNO5. The electrochemical properties were evaluated by Electrochemical Impedance Spectroscopy (EIS) in order to evaluate the electrochemical performances of the cathode material in the presence of the interfacial layer introduced.

I. Experimental part

II.1. Preparation and characterization of the cathode material.

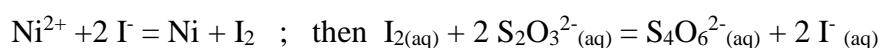
The nitrate-citrate method previously reported by Ferkhi *et al.* [26] was used for the preparation of the $\text{La}_{1.5}\text{Nd}_{0.3}\text{Pr}_{0.2}\text{NiO}_{4+\delta}$ material (LNPNO5). The used precursors were La_2O_3 (Biochem), $\text{Nd}(\text{NO}_3)_3 \cdot 6\text{H}_2\text{O}$ (99,0 %, Sigma-Aldrich), $\text{Pr}(\text{NO}_3)_3 \cdot 6\text{H}_2\text{O}$ (99,9 %, Sigma- Aldrich), and $\text{Ni}(\text{NO}_3)_2 \cdot 6\text{H}_2\text{O}$ (97,0 %, Sigma-Aldrich). After the complete dissolution of the metal cations in nitric aqueous solution, the addition of citric acid ($\text{C}_6\text{H}_8\text{O}_7$) in slight excess leads to the formation of a gel. This gel (viscous mixture) was then dried at 175 °C, the obtained meringue

was crushed and heated in air at several temperatures, 350 and 500 °C for 1 hour, and finally at 1000 °C for 4 hours.

X-Ray diffraction diagrams were obtained using an XPERT-PRO-type diffractometer (CuK α radiation ($\lambda = 1.5406 \text{ \AA}$). The refinement of the diffraction spectra was performed using the "JANA" software, which allows for determining the structural cell parameters.

The morphology and microstructure of the powders and pellets were studied using a JEOL / EO version 1.07 Scanning Electron Microscope.

For the purpose of estimating oxygen stoichiometry, iodometric titration was used according to the following experimental protocol: a mass of the material ($\approx 100 \text{ mg}$) was dissolved in a potassium iodide solution ($10^{-2} \text{ mol.L}^{-1}$) and concentrated hydrochloric acid (HCl, 12 mol.L^{-1}) at 60 °C, under Ar flow. Once in solution, the Ni cations were reduced by the iodide ions (I^-), and the amount of generated iodine is then dosed with sodium thiosulphate ($\text{Na}_2\text{S}_2\text{O}_3$, $10^{-2} \text{ mol.L}^{-1}$) in the presence of a few drops of starch as indicator dye, according to the following two reactions:



The XPS analysis was carried out to study the elemental surface composition and the oxidation states of various elements constituting the surface of the prepared material. The measurements were carried out on a Thermo Fisher K-Alpha spectrometer using a monochromatic Al K α X-ray beam (1486.6 eV, 300 μm spot size). Surface charge effects were avoided using an electron flood gun. The pressure in the analyzer chamber was about $2 \times 10^{-8} \text{ Pa}$. The survey spectra were recorded with a pass energy of 200 eV and, for high-resolution spectra, this energy was lowered to 30 eV. Thermo Scientific Advantage software (version 5.943) was used for the collection and processing of the spectra. Binding energy shifts were corrected against the adventitious position of the C 1s carbon set at 284.6 eV and the BE precision was $\pm 0.1 \text{ eV}$.

Excessive reactivity between the different layers of the symmetrical cells can induce the formation of insulating phases leading to an increase in polarization resistance and also to a drastic decrease in ionic transfer at the cathode/electrolyte interface. It was thus important to study the chemical reactivity between the different materials of the cell in order to better optimize the interfaces. For the prepared half-cells, two interfaces "cathode / interfacial layer" and "interfacial layer/electrolyte" were studied. For this purpose, powders of (cathode; interfacial layer) and (interfacial layer; electrolyte) were mixed (mass ratio 1:1) and sintered at 1350 and 800 °C for 3 days, respectively. After this treatment, the powder mixtures were analyzed by the XRD method.

II.2. Preparation of symmetrical half cells

The dense $\text{Ce}_{0.9}\text{Gd}_{0.1}\text{O}_{1.95}$ (GDC10) pellet was prepared by isostatic pressing at 3000 bar for 5 min, then sintered for 10 h at 1400 °C [27]. The electrolyte pellet had finally a diameter of ~ 16 mm, a thickness of ~ 1.5 mm, and a density higher than 95% of the theoretical value. Regarding the interfacial layer composed of 50% $(\text{ZrO}_2)_{0.92}(\text{Y}_2\text{O}_3)_{0.08}$ (8YSZ) and 50% GDC10 (so-called GDC-YSZ), it was prepared by mixing the two powders (8YSZ and GDC10), and ground together in a mortar, then, mixed with water and methyl cellulose [28, 29] to form a homogeneous ink (powders in suspension), avoiding any agglomeration. After stirring for 12 h, this ink was symmetrically deposited, as uniformly as possible, on the two sides of the previously prepared pellet of the GDC10 electrolyte, using a fine brush cleaned beforehand with distilled water and ethanol. Sintering at 1350 °C /1 hour was necessary to obtain good adhesion between the (GDC-YSZ) layer and the electrolyte [30]. After the final sintering of the interfacial layer, the cathode material layer was prepared and deposited using the same method.

II.3. Electrochemical Impedance Spectroscopy measurements

Electrochemical Impedance Spectroscopy (EIS) measurements were carried out under a single air atmosphere to characterize symmetrical half-cells including the GDC-YSZ interfacial layer added between the cathode material and the GDC10 electrolyte.

The symmetrical cells (Pt/electrolyte/Pt), (interfacial layer/electrolyte/interfacial layer) and (cathode/interfacial layer/electrolyte/interfacial layer/cathode) were placed in a high-temperature oven ($T_{\text{max}} = 850$ °C) between two current collectors made of Pt grids. The EIS measurements were performed in a four-electrode configuration under zero current conditions using an Autolab 72739 equipped with a Frequency Response Analyzer (FRA), in the range of 0.01 Hz to 1 MHz with an applied amplitude of 50 mV (a linear response was observed for amplitudes varying from 50 to 300 mV). The impedance diagrams were analyzed using Zview software [27]. It should be noted that for the cells without the nickelate cathode, a platinum layer (Platinum ink 6082, METALOR ®) was deposited by painting using a fine brush in a symmetrical manner on both sides of the cell and heated in air at 900 °C, for 1 hour, before EIS measurements to improve the electrical contacts.

III. Results and Discussion

III.1. X-Ray Diffraction (XRD)

The XRD diagram obtained at room temperature for the LNPNO5 powder calcined at 1000 °C for 4 hours (**Figure 1**) characterizes a pure and well-crystallized sample. The peaks are indexed using the JCPDS sheet # 211274. The results found are in good agreement with the results found previously by Vibhu, Vaibhav, et al. [31] when studying the $\text{La}_{1.5}\text{Pr}_{0.5}\text{NiO}_{4+\delta}$ composition and in agreement with the results of the $\text{La}_{1.5}\text{Pr}_{0.5}\text{NiO}_{4+\delta}$ and $\text{La}_{1.5}\text{Pr}_{0.5}\text{Ni}_{0.9}\text{Cu}_{0.1}\text{O}_4$ compounds reported by Zhao, Chen, et al [32].

The lanthanum-based compound ($\text{La}_{1.5}\text{Nd}_{0.3}\text{Pr}_{0.2}\text{NiO}_{4+\delta}$) doped with neodymium (Nd) and praseodymium (Pr) crystallizes in an orthorhombic structure with the Fmmm space group [31,33-35]. The determined cell parameters are: $a = 5,4451 \text{ \AA} (\pm 0.01 \text{ \AA})$, $b = 5,4719 \text{ \AA} (\pm 0.01 \text{ \AA})$, $c = 12,6137 \text{ \AA} (\pm 0.002 \text{ \AA})$, $\alpha = \beta = \gamma = 90^\circ$ and the cell volume = $375,827 \text{ \AA}^3 (\pm 0.0001 \text{ \AA}^3)$. As expected, doping with an element with a lower radius such as praseodymium and neodymium compared to that of lanthanum leads to a decrease in the lattice parameters (radii $\text{La}^{3+} = 1.032 \text{ \AA} > \text{radii Pr}^{3+} = 0.990 \text{ \AA} > \text{radii Nd}^{3+} = 0.983 \text{ \AA}$ [36]), which has already been observed and discussed by other authors [36, 37].

III.2. Scanning Electron Microscopy

Figure 2 shows the SEM image obtained for LNPNO5, we observe the simultaneous presence of agglomerates consisting of small grains (submicron) of spherical shape with a grain size of 300 nm approximately.

The SEM image recorded for the cross-section of the LNPNO5/GDC-YSZ/GDC/GDC-YSZ/LNPNO5 and LNPNO5/GDC/LNPNO5 symmetrical cells is shown in **Figure 3. a** and **b** respectively. It should be noted that sample preparation for this observation is a delicate step, as manually breaking the cell in half leads to the phenomenon of wiping the surface layer of LNPNO5 and sometimes to fissures in the GDC electrolyte (cells do not break in two regularly). The thickness of the interfacial layer is of the order of 6 μm and it is quite clear that the interfacial layer and the electrode are homogeneous and well adhering to both the electrolyte and cathode materials, which is supposed to lower the interface polarization resistances, resulting in an improvement of the electrochemical performances.

III.3. Oxygen stoichiometry (δ) determined by iodometric titration

The δ value determined in this work ($\delta = 0.16$) well agrees with that found by Vibhu *et al.* [31] for the material $\text{La}_{1.5}\text{Pr}_{0.5}\text{NiO}_{4+\delta}$ ($\delta = 0.17$). It is known that oxygen stoichiometric A_2BO_4 compounds have strong structural constraints; the insertion of additional oxygen within the structure and the partial oxidation of divalent into trivalent nickel are two phenomena that

contribute to the stabilization of the structure. The doping of the lanthanum site with elements of smaller ionic radii increases steric stresses, leading to favor an increase in oxygen over-stoichiometry. **Table 1** illustrates oxygen stoichiometry values measured at 25° C in previous works. Since the Pr³⁺ and Nd³⁺ have close ionic radii, it is then logical to reach similar δ values.

Table 1. Oxygen over-stoichiometry values measured at 25 °C for various A₂BO₄ compounds.

Sample	Method of Elaboration	T °C/Sintering	(δ iod.)	(δ TGA)	Ref.
La _{1.5} Pr _{0.5} NiO _{4+δ}	nitrate-citrate	1200 /2 h	0.17	0.16	[31]
La ₂ Ni _{0.8} Co _{0.2} O ₄	Sol- Gel	/	0.20	/	[38]
La ₂ Ni _{0.7} Co _{0.3} O _{4+δ}	Sol- Gel	1300 /8 h	0.15	/	[39]
La _{1.5} Nd _{0.3} Pr _{0.2} NiO _{4+δ}	nitrate-citrate	1000 /4 h	0.16		This Work

III.4. XPS Analysis

In the XPS spectra of the La_{1.5}Nd_{0.3}Pr_{0.2}NiO_{4.16} powder, all the structural elements are correctly observed on the surface of the synthesized material (**Figure 4**, survey spectrum in the top panel (a)). These elements are the La and Ni, the Nd and Pr dopants, Oxygen, and adventitious carbon (from surface contamination). Figure 4 also displays the details of the oxygen 1s core level (middle panel (b)), and the La-Ni core levels region (bottom panel (c)). This study is focused on the quantification one can extract from the curve fitting of the most significant regions of the spectra, namely the La 3d, Ni 2p, Nd 3d, Pr 3d, and O1s core levels peaks. Atomic percentages of those elements were calculated based on the measured peak areas of the core levels regions and theoretical photoionization cross sections using the Avantage® software, from Thermo Fischer. It should be noted that to minimize fitting errors, the nickel concentration has been calculated using Ni 3p core level peak at 68 eV, instead of the Ni 2p or Ni 3s, because the Ni 2p level is (strongly) overlapped with La 3d_{3/2} one, while the Ni 3s line is overlapped with La 4p one.

The XPS experimentally determined elemental composition is summarized in **Table 2**, which also reports the expected values (or theoretical values) that have been theoretically calculated from the nickelate formula.

Table 2. XPS quantification of the surface composition of the $\text{La}_{1.5}\text{Nd}_{0.3}\text{Pr}_{0.2}\text{NiO}_{4.16}$ material; the theoretical values are calculated from the nickelate formula.

Element	La	Ni	Pr	Nd	O	La + Pr + Nd	$\frac{\text{O}_{\text{latt}}}{\Sigma \text{ cation}}$	$\frac{\text{O}_{\text{latt}}}{\text{O}_{\text{ads}}}$	$\text{O}_{\text{ads(OH)}}\%$
						Ni			
XPS values (%)	10.0	14.3	0.8	3.7	43.8	1.0	0.7	0.65	24.68
Theoretical values / (%)	21.0	14.0	2.8	4.2	58.1	2.0	1.4		

The O 1s region, as examined earlier [5], contains three types of oxygen atoms, with different local chemical environments (**Figure 4b**); the peaks at 528.4 eV and 529.9 eV fingerprint the oxygen of the crystal lattice; at 531.0 eV are the oxygen atoms of hydroxyl groups, while the 532.4 eV peak identifies the oxygen type corresponding to adsorbed water [40-44]. According to the curve fitting results, the oxygen atoms in the crystal lattice account for 16.2 % of the total material composition, whereas hydroxyl groups and water account for 25.1 % and 2.4 %, respectively. As shown in **Table 2**, the nickelate surface is strongly hydroxylated (OH^-); this is a property of most rare earth oxide materials that can be identified thanks to the surface sensitivity of the XPS analysis.

Table 2 allows comparing the surface composition measured by XPS and the calculated one by supposing a stoichiometric material composition. Note that the carbon superficial contamination is not shown in the table, but has been included in the calculations. Note also that if the nickel element surface concentration has not significantly changed, the rest of the elements have lower values than those expected. Clear differences appear thus between the surface composition and the expected values.

The calculated ($\text{O}_{\text{latt}} / \Sigma \text{ cations}$) ratio between the oxygen of the lattice and the sum of all the cations is half of the expected amount, the results show that the lattice oxygen content at the surface (0.7) is slightly lower than that of the bulk, indicating a cationic character of the surface of LNPNO5 material. This may enhance the surface activity of the materials. On the other hand, due to the coexistence of Ni(II) and Ni(III) on the surface of LNPNO5 material, the cationic redox reaction, surface charge storage as well as electronic and ionic properties can also be improved.

Being around 57.2% of the total surface oxygen, the quantity of the surface hydroxyls surpasses all the other oxygen species. It is therefore quite possible that the OH^- comes from the hydroxylation of some cations, in particular, the lanthanide elements of the La, Nd, and Pr

owing to their hygroscopic nature, as well as from the conversion of part of the lattice oxygen into hydroxyl groups. One knows indeed that some water is adsorbed on the material surface. In **Figure 4c**, the La(3d) and Ni(2p) XPS region is complex due to strong overlapping caused by spin-orbit effects, shake-up satellites, and chemical shifts. Indeed, one very interesting observation is that the La 3d_{3/2} + Ni 2p_{3/2} region, in the lanthanum nickelate oxides, has a distinct shape when compared to Ni-free lanthanide compounds. In the first ones, the region appears much broader and the intensity of the main peak of La 3d_{3/2} is lower than that of the presumed satellite peak; this is undoubtedly due to the real contribution of Ni 2p_{3/2} components. In this work, we point out that the La_{1.5}Nd_{0.3}Pr_{0.2}NiO_{4.16} material has a particular composition due to the presence of one transition metal and three lanthanide elements. These four elements form ionic bonds with the oxygen anions [45] and therefore the binding energies of their core levels should show high values. But the lanthanum element is partially substituted by 25% of two other lanthanide elements, Nd and Pr. This is expected to reduce the ionic character of the La-O bond and allow the binding energy of La 3d_{3/2} to be displaced to a lower value. In addition to this, it was recently revealed that in the lanthanum nickelate perovskite compound, the Ni-O bond has a stronger ionic character than the La-O bond [46]. This also makes it possible to predict a displacement of the positions of the Ni 2p_{3/2} components to the high values while the La 3d_{3/2} components will shift to the low values. Accordingly, this can be considered as somewhat facilitating the separation of the Ni 2p_{3/2} and La 3d_{3/2} components in the La 3d_{3/2} + Ni 2p_{3/2} region.

Then one can safely identify between 845 and 858 eV four main components: at lower binding energy (849.6 eV and 851.2 eV) are two peaks attributed to La 3d_{3/2}, while at higher binding energy (853.7 eV and 855.1 eV) two structures can be assigned to the Ni²⁺ and Ni³⁺ components, of the 3/2 spin-orbit doublet [41, 43, 44, 46]. It is observed that the Ni³⁺ oxidized species are the most contributory by about 57% which can even be balanced with oxygen super-stoichiometry and may have a role in ensuring the chemical stability of the surface material.

The percentages of XPS and theoretical calculations in **Table 2** reveal that the sum of the XPS quantity of lanthanides is roughly half of the expected value and is close to the nickel amount in the surface, while the nickel quantity is practically unaltered. This indicates that the surface of the material is rich in nickel in comparison to the lanthanides.

The calculated ($O_{\text{lat}}/\Sigma\text{cations}$) ratio and Ni³⁺ percentage are parameters indicating that the surface is rich in cations (compared to anions) suggesting the material surface has a cationic character, or rather it has some properties of a Lewis acid. Through this surface study, it can

be concluded that the surface of the material has undergone a drastic change after the introduction of Nd and Pr elements. In the next paragraphs, we will show this ‘Lewis acid’ property may be reflected in good electrochemical characteristics.

III.5. Chemical Reactivity

It should be noted that the temperatures chosen for the studies of the chemical reactivity between the various components of the symmetrical cells correspond to the heat treatment temperatures for subsequent shaping.

III.5.1. Chemical reactivity between the interfacial layer (IL) and the electrolytes

The chemical reactivity between the two electrolytes (8YSZ and GDC10) was studied through the study of the thermal behavior of the GDC-YSZ mixture (50% (YSZ) / 50% (GDC10)). **Figure 5** shows the diffractograms of the electrolytes 8YSZ, GDC10, and of the GDC-YSZ mixture obtained after heating at 1350 °C during 3 days. From **Figure 5a**, only the peaks characterizing the two phases 8YSZ and GDC10 are observed [28-30]. The reactivity test between the two electrolytes, 8YSZ and GDC10, (**Figure 5b**) shows that both compounds retain their own structure without any significant chemical reaction. Obviously, no new peak is identified in the XRD diagram, indicating that there is no chemical reaction between them at least under the conditions of this work.

III.5.2. Study of the reactivity between the Interfacial Layer (IL) and the electrode

A mixture of 50/50 (% wt) of the LNPNO5 and GDC-YSZ powders was heated at 800 °C during 3 days, in air. Their XRD diffractogram is represented in **Figure 6**.

This experiment was performed in order to check a possible decomposition of the LNPNO5 phase leading to the formation of secondary phases as previously observed for similar nickelates [28]. From Figure 6, no structural changes were found, which is in agreement with Solis *et al.* [47] who did not report any decomposition of the $\text{La}_{1.5}\text{Pr}_{0.5}\text{NiO}_{4+\delta}$ powder after 2 weeks at 750 °C, in air, attesting to the absence of any decomposition or reactivity with the electrolyte. The LNPNO5 material exhibits good thermodynamic stability at an intermediate operating temperature of 800 °C. Both interfaces of our cells are well optimized, and electrochemical studies can be performed on the corresponding cells prepared in these conditions. This mixture, therefore, can be used as an interfacial layer between the $\text{La}_{1.5}\text{Nd}_{0.3}\text{Pr}_{0.2}\text{NiO}_{4.16}$ material and the $\text{Ce}_{0.9}\text{Gd}_{0.1}\text{O}_{2-\delta}$ electrolyte.

III.6. Electrochemical characterizations

With the goal to characterize the electrochemical properties of the ceramic cells, Electrochemical Impedance Spectroscopy (EIS) measurements were performed. In addition, in order to distinguish the different impedance contributions of the various components of the cell (electrolyte, interfacial layer, and the electrode), the electrochemical measurements were performed under air versus temperature on the following symmetrical cells: Pt/ GDC-YSZ /GDC10/ GDC-YSZ /Pt and LNPNO5 / GDC-YSZ / GDC10 / GDC-YSZ / LNPNO5.

First of all, it should be noted that the data relating to the electrochemical impedance measurements corresponding to the Pt/GDC/Pt cells published by the same author, M. FERKHI and . al [3] have been reused in this work.

Platinum electrodes and single-phase electrolytes were first measured so that the impedance contribution of the pure ionic conductor can easily be distinguished compared to Pt-blocking electrodes. According to such measurements, the ionic conductivity can be deduced; it is consistent with values previously reported in the literature [28, 48, 49]. For example, the value measured in air, at 700 °C is of the order of 58.9 mS.cm⁻¹ (see Fig.9).

In the same way, EIS diagrams were recorded on the Pt /GDC-YSZ /GDC10 /GDC-YSZ / Pt symmetrical cell. **Figure 7a** and **7b** shows the plots of the Nyquist diagrams recorded at 400 and 700 °C under air. The corresponding equivalent circuit is also presented.

At 400 °C, the impedance diagrams can be decomposed into various contributions that were fitted to the equivalent circuit of type (R1//CPE1)-(R2//CPE2) (as described in the inset of Figure 7a) and at 700 °C to a circuit of type (R1//CPE1).

Based on the Nyquist diagrams observed at low temperatures (400 °C), the different semi-circles characterizing the different phenomena can be attributed as follows:

- The two semi-circles located between 10⁶-10⁴ Hz (HF1) and 10⁴ -10³ Hz (HF2), expressed by the conduction of O²⁻ ions in the grains, are attributed to grains (intra-granular conduction) and grain boundaries (inter-granular conduction) responses respectively [3]. The semi-circle at high frequency (HF1) disappears with increasing temperature.

- The semi-circles appearing between 10³-10¹ Hz show the response of the interfacial layer which ends with the response of a Pt electrode playing the role of a blocking electrode (**Fig.7.a**). With respect to the frequency range and the associated capacitive effect, the resistance R1 can be assigned to the sum of the ohmic resistances of the GDC10 electrolyte and the GDC-YSZ interfacial layer (**Fig.7a**).

The region where the interfacial layer appears is the same in the presence of the LNPNO5 electrode (**Fig. 10.a**).

At high temperature (700 °C), a response shift from the interfacial layer to the medium frequency region can be distinguished. At these temperatures, the kinetics are enhanced and the response of the LNPNO5 electrode becomes increasingly clearer. At 700 °C, the response of LNPNO5 is observed between 10 and 10⁻² Hz (**Fig. 10b**).

To confirm the response of all contributions relating to the electrolyte, interfacial layer, and electrode, the equivalent capacitance of each contribution was calculated using the relations:

$$C_{eq} = R \left(\frac{1-n}{n} \right) \times (CPE)^{1/n}$$

The equivalent capacitances (CPE) of each impedance contribution are plotted as a function of temperature using Schouler's method [50, 51] in **Figure 8**. Nevertheless, the attribution of chemical and/or electrochemical processes is not straightforward.

As shown in **Fig. 8 a and b**, the capacitances of each process do vary slightly with the inverse of the temperature. For the semi-circle at high frequency (HF1), the capacitance values of the GDC electrolyte are around the order of 10⁻⁴ F. cm⁻² (**Fig.8.a**). The capacitances at medium frequencies for the GDC (**Fig.8.a**) and the values concerning the interfacial layer (**Fig.8.b**) are almost of the same order and are between 10⁻³ and 10⁻⁴ F. cm⁻². Depending on the inverse of the temperature, these values vary in increasing ways. This confirms the good localization in the frequency ranges shown below of the responses of the GDC electrolyte (10⁶-10⁴ Hz) and the interfacial layer (from 10³ to about 10⁻¹ Hz).

As for the electrode (**Fig.8.c**), the low-frequency range (LF) is characterized by high capacitance values $C \approx 10^{-1} - 10$ F. cm⁻², it is almost independent of the temperature, which means that the same electrode phenomenon is involved. L. Mogni *et al.* [52], S. Pang *et al.* [53], B. Philippeau *et. al.* [28], and other works [54, 55] have attributed this contribution to the diffusion of O₂ gas through the porous electrode (*i.e.* electrode phenomena).

For the medium frequency (MF) contributions (**Fig.8.c**), the capacitance values correspond to $C \approx 10^{-3} - 10^{-2}$ F.cm⁻², the values being again independent of temperature. By comparison with previous work [29], an increase in the capacitance values (MF) has been noticed, which can be related to the presence of the interfacial layer between the electrode and the electrolyte. This increase in capacitance values has already been observed for instance by T. Ogier *et. al.* [29],

when studying Ln_2NiO_4 (Ln: La, Pr where Nd) materials screen printed on the YSZ electrolyte coated with an interfacial layer of GDC. This capacitance range is attributed to the Oxygen Reduction Reaction (ORR) processes, *i.e.* the phenomena of molecular oxygen dissociation and the charge transfer occurring at the electrode interface/ O_2 gas, rather than ion transfer at the electrode/layer interfacial [56-58].

The O^{2-} ionic conductivities are plotted in **Figure 9** as a function of the inverse of the temperature for the only GDC10 electrolyte and for GDC10 coated with the GDC-YSZ interfacial layer. For comparison, ionic conductivity values of the YSZ electrolyte are also given.

As expected, the ionic conductivity of the ceramic coated with the mixed additional interfacial layer is located between the two single-phase electrolyte materials. As a consequence, the strategy is not to directly reduce the ohmic drop through the electrolyte but to induce a positive effect concerning the ionic transfer at the electrode/electrolyte interface and a beneficial influence on the kinetics of the electrochemical reaction at the level of the electrode material. In order to correlate the electrochemical performances with the architecture of the cell, it is important to consider the effective active surface area. This area is the surface zone where the ionic transfer is possible and can be defined using the concept of constriction resistance. In the case of an ideal situation, the total geometric area can be considered. For a non-ideal situation, the observed resistance (R_{observed}) depends on the real active area. In the present study, considering a constant conductivity (σ) at a fixed temperature, it could be deduced that the GDC-YSZ layer improves the active area between electrode and electrolyte inducing a lower resistance (indeed the conductivity is defined as: $\sigma = 1/R_{\text{observed}} \times (L/A_{\text{active}})$ with L being the thickness). The important information is that GDC conducts the current on the entire surface due to its interface properties.

Electrochemical properties were then performed on LNPNO5 / GDC-YSZ / GDC10 symmetrical cells, made up of the electrode material, the GDC10 electrolyte in the presence of the GDC-YSZ interfacial layer between the cathode and the electrolyte. **Figure 10** shows typical Nyquist diagrams, with the corresponding equivalent circuits, recorded at 400, 500, 600, 700, and 800 °C, in air.

According to the EIS measurements, the Area Specific Resistance (ASR, in $\Omega\cdot\text{cm}^2$) of the LNPNO5 cathode material was calculated using the following relation: $\text{ASR} = R_p \times S / 2$, with R_p , the electrode polarization resistance (R_p) corresponding to the sum of the resistances of the last two semicircles expressed in ohm (Ω), S is the surface area of the sample in cm^2 .

Figure 11 shows the Arrhenius plots of the ASR of LNPNO5 cathode material deposited on the GDC10 electrolyte in the presence of the (YSZ - GDC) interface layer.

It is clearly seen that the addition of the GDC-YSZ interfacial layer between the LNPNO5 cathode material and the GDC10 electrolyte leads to low values of ASR. For example, at 600 °C and 700 °C the ASRs values, 0.060 and 0.022 $\Omega\cdot\text{cm}^2$, respectively, are quite interesting compared to results recently reported in the literature (**Table 3**). The activation energy of the LNPNO5 material is very low and is of the order of 0.96 eV. This phenomenon could be assigned to the improvement of the increase of the electrode/electrolyte surface area. To our knowledge, such low values had never been observed until now on materials of the same family.

Table 3. ASRs values and activation energies of the cathode materials on 8YSZ and GDC electrolytes (this work) compared with those reported in the literature.

Symmetrical cell	Rp ($\Omega\cdot\text{cm}^2$)/T (°C)	Ea (eV)	Ref, Year
On YSZ electrolyte			
La ₂ NiO ₄ / 8YSZ	0.370 /800 °C	1.40	[29], 2015
La ₂ NiO ₄ / 8YSZ	0.930 /600 °C	-	[31], 2015
La ₂ NiO ₄ (Porous) /La ₂ NiO ₄ (dense)/ 8YSZ	2.200 /800 °C	-	[59], 2009
La ₂ NiO ₄ (Porous) /La ₂ NiO ₄ (dense)/GDC /8YSZ	1.300 /800 °C	-	[59], 2009
La ₂ NiO ₄ /Ce _{0.8} Gd _{0.2} O _{2-δ} / 8YSZ	0.090 /800 °C	-	[29], 2015
La _{1.5} Pr _{0.5} NiO ₄ / 8YSZ	0.730 /600 °C	-	[31], 2015
La _{0.5} Pr _{1.5} NiO ₄ / 8YSZ	0.230 /600 °C	-	[31], 2015
LaPrNiO ₄ / 8YSZ	0.290 /600 °C	-	[31], 2015
Pr ₂ NiO _{4+δ} / 8YSZ	0.150 /600 °C	-	[31], 2015
Pr ₂ NiO _{4+δ} / 8YSZ	0.140 /800 °C	0.90	[29], 2015
Nd ₂ NiO _{4+δ} /8YSZ	0.150 /800 °C	1.27	[29], 2015
La _{0.6} Sr _{0.4} Fe _{0.8} Co _{0.2} O ₃ / 8YSZ	0.050 /800 °C	1.53	[29], 2015
Pr ₂ NiO _{4+δ} /Ce _{0.8} Gd _{0.2} O _{2-δ} / 8YSZ	0.050 /800 °C	-	[29], 2015
Nd ₂ NiO _{4+δ} /Ce _{0.8} Gd _{0.2} O _{2-δ} /8YSZ	0.090 /800 °C	-	[29], 2015
La _{0.6} Sr _{0.4} Fe _{0.8} Co _{0.2} O ₃ /Ce _{0.8} Gd _{0.2} O _{2-δ} / 8YSZ	0.050 /800 °C	-	[29], 2015
Pr _{0.5} Ba _{0.5} Co _{0.25} Fe _{0.75} O _{3-δ} /Ce _{0.9} Gd _{0.1} O _{3-δ} /SCSZ	0.050 /700 °C	1.15	[60], 2018
La _{0.6} Sr _{0.4} Fe _{0.9} Nb _{0.1} O _{3-δ} /Ce _{0.8} Gd _{0.2} O _{2-δ} /8YSZ	0.050 /800 °C 0.030 /850 °C	1.56	[61], 2019
On GDC electrolyte			
La ₂ NiO ₄ / GDC	2.200 /600 °C	-	[28], 2013
La ₂ NiO ₄ / GDC	3.330 /600 °C	0.77	[37], 2017
La ₂ NiO ₄ (Porous)/La ₂ NiO ₄ (dense)/ GDC	0.420 /600 °C	1.09	[37], 2017
La _{1.5} Nd _{0.3} Pr _{0.2} NiO _{4.16} /C (50%) + Y (50%)/ GDC	0.060 /600 °C 0.022 /700 °C	0.96	This Work
La _{1.5} Pr _{0.5} NiO ₄ / GDC	2.370 /600 °C	0.63	[37], 2017

LaPrNiO ₄ / GDC	1.630 /600 °C	0.63	[37], 2017
Pr ₂ NiO _{4+δ} / GDC	0.830 /600 °C	0.66	[37], 2017
Pr ₂ NiO _{4+δ} / GDC	0.280 /600 °C	-	[28], 2013
Nd ₂ NiO _{4+δ} / GDC	4.900 /600 °C	-	[28], 2013
La _{1,5} Pr _{0,5} NiO ₄ (Porous)/La _{1,5} Pr _{0,5} NiO ₄ (dense)/ GDC	0.230 /600 °C	1.08	[37], 2017
LaPrNiO ₄ (Porous)/ LaPrNiO ₄ (dense)/ GDC	0.120 /600 °C	0.80	[37], 2017
Pr ₂ NiO _{4+δ} (Porous)/ Pr ₂ NiO _{4+δ} (dense)/ GDC	0.080 /600 °C	0.78	[37], 2017

Indeed, it is interesting to compare our results found for the material LNPNO5 (ASR of 0.06 Ω.cm² (on GDC10 at 600 °C) and activation energy of 0.96 eV) with those reported in Table 3; the combined improvement of conduction and ionic transfer properties, as well as the electrochemical properties of the LNPNO5 cathode material itself, seems to be at the origin of these interesting results and validate the approach of architecture electrode and the choice of LNPNO5 oxide.

III. Conclusion

In this work, a new electrode made of the La_{1,5}Nd_{0,3}Pr_{0,2}NiO_{4,16} material was synthesized by the citrate method and characterized by XRD, SEM, XPS, and iodometric analysis to evaluate the purity of the phase, the morphology of the powders, the surface chemical state and the oxygen (over)stoichiometry, respectively. With the aim of possible use as cathode material for SOFC fuel cells (IT-SOFS), a commercial electrolyte (Ce_{0,9}Gd_{0,1}O_{2-δ} (GDC10) was used, and the interface between the cathode materials and the electrolytes has been improved by the addition of an interfacial layer of composition [8YSZ (50%) + GDC10 (50%)].

The XRD analysis confirmed the purity of the synthesized phases; the materials doped with praseodymium show no other phase, unlike most of the research on these materials which, always, shows the presence of the Pr₆O₁₁ impurity.

The SEM cross-section image shows the good adhesion between the constituents of the cell, a good porosity of the cathode material, the interfacial layer, and the GDC10 electrolyte to be dense. The XPS and iodometry analyses characterize an anionic character of the material, an important property for easy displacement of oxide ions in these materials.

The chemical reactivity was studied between the interfacial layer and GDC10 electrolyte and, also, between the synthesized material and (8YSZ (50%) + GDC10 (50%)) interfacial layer.

The XRD diagram showed no impurity phase meaning no chemical reactivity between all the cathode and electrolyte components.

The electrochemical measurements by impedance spectroscopy (EIS) of the symmetrical half-cell show $\text{La}_{1.5}\text{Nd}_{0.3}\text{Pr}_{0.2}\text{NiO}_{4.16}$ specific resistance values in the presence of the interfacial layer (8YSZ (50%) + GDC10 (50%)) as low as $0.06 \Omega\cdot\text{cm}^2$ at $600 \text{ }^\circ\text{C}$ and $0.022 \Omega\cdot\text{cm}^2$ at $700 \text{ }^\circ\text{C}$. It has been concluded that this material exhibits very good electrochemical properties at the intermediate temperature of 600 and $700 \text{ }^\circ\text{C}$; this confirms the interest in such a new architecture (consisting of this new material in the presence of the new interfacial layer) at intermediate temperatures for SOFCs. The activation energy of the LNPNO5 material is 0.96 eV meaning the improvement of the kinetics of the reactions at the level of the electrode. It was also observed that the capacitance values were increased compared to the literature values due to the benefit of the presence of the interfacial layer between the electrode and the electrolyte.

We finally demonstrated an interest in structured cells made up of an interface layer based on GDC and YSZ; in addition, $\text{La}_{1.5}\text{Nd}_{0.3}\text{Pr}_{0.2}\text{NiO}_{4.16}$ can be qualified to be an excellent cathode material for SOFC fuel cells operating at intermediate temperatures, $600 - 700 \text{ }^\circ\text{C}$.

IV. Declarations

Ethical Approval

we confirm that this work has no conflicts of interest with any institution or person and the work ensures that no act of plagiarism exists.

Competing interests

We ensure that there are no conflicts of interest with scientific or other institutions or persons.

Authors' contributions

The authors confirm their contribution to the paper as follows: study conception and design: S. Amira, S. Fourcade. Data collection: S. Amira, M. Ferkhi; analysis and interpretation of results: M. Ferkhi, F. Mauvy, S. Fourcade, J.M. Bassat, J.C. Grenier; draft manuscript preparation: S. Amira. M. Ferkhi. All authors reviewed the results and approved the final version of the manuscript.

Funding

We confirm that we have mentioned our affiliations and we confirm that no institution has funded this work.

Availability of data and materials

Any datasets used can be accessed.

V. References

- [1] V. S. Arunachalam, E. L. Fleischer, The Global Energy Landscape and Materials Innovation. *MRS Bulletin* 33, 264–288 (2008). <https://doi.org/10.1557/mrs2008.61>
- [2] M. Ferkhi, S. Khelili S, L. Zerroual, A. Ringuedé, M. Cassir, Synthesis, structural analysis and electrochemical performance of low-copper content $\text{La}_2\text{Ni}_{1-x}\text{Cu}_x\text{O}_{4+\delta}$ materials as new cathodes for solid oxide fuel cells. *Electrochimica acta* 54, 6341-6346 (2009). <https://doi.org/10.1016/j.electacta.2009.05.082>
- [3] M. Ferkhi, A. Ringuedé, A. Khaled, L. Zerroual, M. Cassir, $\text{La}_{1.98}\text{NiO}_{4+\delta}$, a new cathode material for solid oxide fuel cell: Impedance spectroscopy study and compatibility with gadolinia-doped ceria and yttria-stabilized zirconia electrolytes. *Electrochimica acta* 75, 80-87 (2012). <https://doi.org/10.1016/j.electacta.2012.04.064>
- [4] M. Ferkhi, H. Ahmed Yahia, Electrochemical and morphological characterizations of $\text{La}_{2-x}\text{NiO}_{4+\delta}$ ($x = 0.01, 0.02, 0.03$ and 0.05) as new cathodes materials for IT-SOFC. *Materials Research Bulletin* 83, 268-274 (2016). <https://doi.org/10.1016/j.materresbull.2016.06.009>
- [5] S. Amira, M. Ferkhi, A. Khaled, F. Mauvy, J.C. Grenier, L. Houssiau, J.J. Pireaux, Carbon-based lanthanum nickelate material $\text{La}_{2-x-y}\text{Nd}_x\text{Pr}_y\text{NiO}_{4+\delta}$ ($x = 0, 0.3$, and 0.5 ; $y = 0$ and 0.2) as a bifunctional electrocatalyst for oxygen reduction in alkaline media. *Ionics* 25, 3809-3822 (2019). <https://doi.org/10.1007/s11581-019-02963-0>
- [6] D. Marinha, J. Hayd, L. Dessemond, E. Ivers-Tiffée, E. Djurado, Performance of $(\text{La}, \text{Sr})(\text{Co}, \text{Fe})\text{O}_{3-x}$ double-layer cathode films for intermediate temperature solid oxide fuel cell. *Journal of Power Sources* 196, 5084-5090 (2011). <https://doi.org/10.1016/j.jpowsour.2011.01.063>
- [7] G. Constantin, C. Rossignol, P. Briois, A. Billard, L. Dessemond, E. Djurado, Efficiency of a dense thin CGO buffer layer for solid oxide fuel cell operating at intermediate temperature. *Solid State Ionics* 249, 98-104 (2013). <https://doi.org/10.1016/j.ssi.2013.07.004>
- [8] T. Ogier, New anode materials and architectural cells for high temperature electrolyser. University of Sciences and Technologies-Bordeaux I, Ph.D thesis, (2012).
- [9] B.C.H Steele, J.M. Bae, Properties of $\text{La}_{0.6}\text{Sr}_{0.4}\text{Co}_{0.2}\text{Fe}_{0.8}\text{O}_{3-x}$ (LSCF) double layer cathodes on gadolinium-doped cerium oxide (CGO) electrolytes: II. Role of oxygen exchange and diffusion. *Solid State Ionics* 106, 255-261 (1998). [https://doi.org/10.1016/S0167-2738\(97\)00430-X](https://doi.org/10.1016/S0167-2738(97)00430-X)
- [10] N. Hildenbrand, B.A. Boukamp, P. Nammensma, D.H. Blank, Improved cathode/electrolyte interface of SOFC. *Solid state ionics* 192,12-15 (2011). <https://doi.org/10.1016/j.ssi.2010.01.028>
- [11] K. Dumaisnil K, Elaboration and characterizations of cathode and electrolyte materials for solid oxide fuel cell. Université du Littoral Côte d'Opale, Ph.D thesis,(2015).

- [12] S.P. Simner, J.F. Bonnett, N.L. Canfield, K.D. Meinhardt, J.P. Shelton, V.L. Sprenkle, J.W. Stevenson, Development of lanthanum ferrite SOFC cathodes. *Journal of power sources* 113, 1-10 (2003). [https://doi.org/10.1016/S0378-7753\(02\)00455-X](https://doi.org/10.1016/S0378-7753(02)00455-X)
- [13] M. Shiono M, K. Kobayashi, T.L. Nguyen, K. Hosoda, T. Kato T, K. Ota, M. Dokiya, Effect of CeO₂ interlayer on ZrO₂ electrolyte/La(Sr)CoO₃ cathode for low-temperature SOFCs. *Solid State Ionics* 170,1-7 (2004). <https://doi.org/10.1016/j.ssi.2004.02.018>
- [14] S. Charojrochkul, K.L. Choy, B.C.H. Teele, Cathode/electrolyte systems for solid oxide fuel cells fabricated using flame assisted vapor deposition technique. *Solid State Ionics* 121,107-113 (1999). [https://doi.org/10.1016/S0167-2738\(98\)00536-0](https://doi.org/10.1016/S0167-2738(98)00536-0)
- [15] I. Jang, S. Kim, C. Kim, H. Lee, H. Yoon, T. Song, U. Paik, Interface engineering of yttrium stabilized zirconia/gadolinium doped ceria bi-layer electrolyte solid oxide fuel cell for boosting electrochemical performance. *Journal of Power Sources* 435, 226776 (2019). <https://doi.org/10.1016/j.jpowsour.2019.226776>
- [16] P. Singh, Electrical conductivity of YSZ-SDC composite solid electrolyte synthesized via a glycine-nitrate method. *Ceramics International* 43,11692-11698 (2017). <https://doi.org/10.1016/j.ceramint.2017.05.359>
- [17] M.G. Bellino, D.G. Lamas, N.E. Walsøe de Reça, Preparation and ionic transport properties of YDC–YSZ nanocomposites. *Journal of Materials Chemistry* 18, 4537-4542 (2008). <https://doi.org/10.1039/B807667G>
- [18] H.H. Lim, E. Sulistya, M.Y. Wong, B. Salamatinia, B. Amini Horri, Ceramic Nanocomposites for Solid Oxide Fuel Cells. In: Mishra, A. (eds) *Sol-gel Based Nanoceramic Materials: Preparation, Properties, and Applications*. Springer, Cham. 157-183 (2017). https://doi.org/10.1007/978-3-319-49512-5_6
- [19] S.B. Adler, J.A. Lane, B.C.H. Steele, Electrode kinetics of porous mixed-conducting oxygen electrodes. *Journal of the electrochemical society* 143,3554-3564 (1996). <https://doi.org/10.1149/1.1837252>
- [20] S.B. Adler, Mechanism and kinetics of oxygen reduction on porous La_{1-x}Sr_xCoO_{3-δ} electrodes. *Solid State Ionics* 111, 125-134 (1998). [https://doi.org/10.1016/S0167-2738\(98\)00179-9](https://doi.org/10.1016/S0167-2738(98)00179-9)
- [21] A.V. Berenov, A. Atkinson, J.A. Kilner, E.Bucher, W. Sitte, Oxygen tracer diffusion and surface exchange kinetics in La_{0.6}Sr_{0.4}CoO_{3-δ}. *Solid State Ionics* 181, 819-826 (2010). <https://doi.org/10.1016/j.ssi.2010.04.031>
- [22] I.D. Brown, Modelling the structures of La₂NiO₄. *Zeitschrift für Kristallographie-Crystalline Materials* 199, 255-274 (1992). <https://doi.org/10.1524/zkri.1992.199.3-4.255>
- [23] S.J. Skinner, J.A. Kilner, Oxygen diffusion and surface exchange in La_{2-x}Sr_xNiO_{4+δ}. *Solid State Ionics* 135,709-712 (2000). [https://doi.org/10.1016/S0167-2738\(00\)00388-X](https://doi.org/10.1016/S0167-2738(00)00388-X)

- [24] J.M. Bassat, M. Burriel, O.Wahyudi, R. Castaing, M. Ceretti, P. Veber, J.A. Kilner, Anisotropic oxygen diffusion properties in $\text{Pr}_2\text{NiO}_{4+\delta}$ and $\text{Nd}_2\text{NiO}_{4+\delta}$ single crystals. *The Journal of Physical Chemistry C* 117, 26466-26472 (2013). <https://doi.org/10.1021/jp409057k>
- [25] A. Montenegro Hernández, L. Mogni, A. Caneiro, $\text{La}_2\text{NiO}_{4+\delta}$ as cathode for SOFC: Reactivity study with YSZ and CGO electrolytes. *International Journal of Hydrogen Energy* 35, 6031-6036 (2010). <https://doi.org/10.1016/j.ijhydene.2009.12.077>
- [26] M. Ferkhi M, M. Rekaik, A. Khaled, M. Cassir, J.J. Pireaux, Neodymium nickelate $\text{Nd}_{2-x}\text{Sr}_x\text{Ni}_{1-y}\text{Co}_y\text{O}_{4\pm d}$ (x and $y = 0$ or 0.05) as cathode materials for the oxygen reduction reaction. *Electrochimica Acta* 229, 281-290 (2017). <https://doi.org/10.1016/j.electacta.2017.01.023>
- [27] P. Batocchi, F. Mauvy, S. Fourcade, M. Parco, Electrical and electrochemical properties of architected electrodes based on perovskite and A_2MO_4 type oxides for Protonic Ceramic Fuel Cell. *Electrochimica Acta* 145, 1-10 (2014). <https://doi.org/10.1016/j.electacta.2014.07.001>
- [28] B. Philippeau, F. Mauvy, C. Mazataud, S. Fourcade, J.C. Grenier, Comparative study of electrochemical properties of mixed conducting $\text{Ln}_2\text{NiO}_{4+\delta}$ ($\text{Ln} = \text{La}, \text{Pr}$ and Nd) and $\text{La}_{0.6}\text{Sr}_{0.4}\text{Fe}_{0.8}\text{Co}_{0.2}\text{O}_{3-\delta}$ as SOFC cathodes associated to $\text{Ce}_{0.9}\text{Gd}_{0.1}\text{O}_{2-\delta}$, $\text{La}_{0.8}\text{Sr}_{0.2}\text{Ga}_{0.8}\text{Mg}_{0.2}\text{O}_{3-\delta}$ and $\text{La}_9\text{Sr}_1\text{Si}_6\text{O}_{26.5}$ electrolytes. *Solid State Ionics* 249,17-25 (2013). <https://doi.org/10.1016/j.ssi.2013.06.009>
- [29] T. Ogier, F. Mauvy, J.M. Bassat, J. Laurencin, J. Mougín, J.C. Grenier Overstoichiometric oxides $\text{Ln}_2\text{NiO}_{4+\delta}$ ($\text{Ln} = \text{La}, \text{Pr}$ or Nd) as oxygen anodic electrodes for solid oxide electrolysis application. *International Journal of Hydrogen Energy* 40, 15885-15892 (2015). <https://doi.org/10.1016/j.ijhydene.2015.09.107>
- [30] Q. Li, X. Zeng, L. Sun, H. Zhao, L. Huo, J.C. Grenier, Electrochemical performance of $\text{La}_2\text{Cu}_{1-x}\text{Co}_x\text{O}_4$ cathode materials for intermediate-temperature SOFCs. *International Journal of Hydrogen Energy* 37, 2552–2558 (2012). <https://doi.org/10.1016/j.ijhydene.2011.11.014>
- [31] V. Vibhu, A. Rougier, C. Nicollet, A. Flura, J.C. Grenier, J.M. Bassat. $\text{La}_{2-x}\text{Pr}_x\text{NiO}_{4+\delta}$ as suitable cathodes for metal-supported SOFCs. *Solid State Ionics* 278, 32-37(2015). <https://doi.org/10.1016/j.ssi.2015.05.005>
- [32] C. Zhao, Q. Zhou, T. Zhang, L. Qu, X. Yang, T. Wei. Preparation and electrochemical properties of $\text{La}_{1.5}\text{Pr}_{0.5}\text{NiO}_4$ and $\text{La}_{1.5}\text{Pr}_{0.5}\text{Ni}_{0.9}\text{Cu}_{0.1}\text{O}_4$ cathode materials for intermediate-temperature solid oxide fuel cells. *Materials Research Bulletin* 113, 25-30 (2019). <https://doi.org/10.1016/j.materresbull.2019.01.016>
- [33] E. Boehm, J.M. Bassat, P. Dordor, F. Mauvy, J.C. Grenier, P. Stevens, Oxygen diffusion and transport properties in non-stoichiometric $\text{Ln}_{2-x}\text{NiO}_{4+\delta}$ oxides. *Solid State Ionics* 176, 2717-2725 (2005). <https://doi.org/10.1016/j.ssi.2005.06.033>

- [34] R. Sayers, S.J. Skinner, Evidence for the catalytic oxidation of $\text{La}_2\text{NiO}_{4+\delta}$. *Journal of materials chemistry* 21,414-419 (2011). <https://doi.org/10.1039/C0JM02419H>
- [35] A. Akbari-Fakhrabadi, E.G. Toledo, J.I. Canales, V. Meruane, S.H. Chan, M.A. Gracia-Pinilla, Effect of Sr^{2+} and Ba^{2+} doping on structural stability and mechanical properties of $\text{La}_2\text{NiO}_{4+\delta}$. *Ceramics International* 44,10551-10557 (2018). <https://doi.org/10.1016/j.ceramint.2018.03.077>
- [36] R.D. Shannon, Revised effective ionic radii and systematic studies of interatomic distances in halides and chalcogenides. *Acta crystallographica section A: crystal physics, diffraction, theoretical and general crystallography* 32, 751-767 (1976). <https://doi.org/10.1107/S0567739476001551>
- [37] R.K. Sharma, S.K. Cheah, M. Burriel, L. Dessemond, J.M. Bassat, E. Djurado, Design of $\text{La}_{2-x}\text{Pr}_x\text{NiO}_{4+\delta}$ SOFC cathodes: a compromise between electrochemical performance and thermodynamic stability. *Materials Chemistry A* 5,1120–1132 (2017). <https://doi.org/10.1039/C6TA08011A>
- [38] Y. Huan, S. Chen, R. Zeng, T. Wei, D. Dong, X. Hu, Y. Huang, Intrinsic Effects of Ruddlesden-Popper-Based Bifunctional Catalysts for High-Temperature Oxygen Reduction and Evolution. *Advanced Energy Materials* 9, 1901573 (2019). <https://doi.org/10.1002/aenm.201901573>
- [39] C.N. Munnings, S.J. Skinner, G. Amow, P.S. Whitfield, I.J. Davidson, Oxygen transport in the $\text{La}_2\text{Ni}_{1-x}\text{Co}_x\text{O}_{4+\delta}$ system. *Solid State Ionics* 176, 1895-1901 (2005). <https://doi.org/10.1016/j.ssi.2005.06.002>
- [40] M. Wei, W. Che, H. Li, Z. Wang, F. Yan, Y. Liu, J. Liu, Ruddlesden-Popper type $\text{La}_2\text{NiO}_{4+\delta}$ oxide coated by Ag nanoparticles as an outstanding anion intercalation cathode for hybrid supercapacitors. *Applied Surface Science* 484, 551-559 (2019). <https://doi.org/10.1016/j.apsusc.2019.04.015>
- [41] W. Che, M. Wei, Z. Sang, Y. Ou, Y. Liu, J. Liu, Perovskite $\text{LaNiO}_{3-\delta}$ oxide as an anion-intercalated pseudocapacitor electrode. *Journal of Alloys and Compounds* 731, 381-388 (2018). <https://doi.org/10.1016/j.jallcom.2017.10.027>
- [42] L. Mao, Y. Yan, X. Zhao, M. Fu, Y. Xiao, G. Dong, Comparative study on removal of NO_x and soot with a-site substituted La_2NiO_4 perovskite-like by different valence cation. *Catalysis Letters* 149, 1087-1099 (2019). <https://doi.org/10.1007/s10562-019-02690-1>
- [43] Y. Wu, T. Wang, Y. Zhang, S.Xin, X. He, D. Zhang, J. Shui, Electrocatalytic performances of g- C_3N_4 - LaNiO_3 composite as bi-functional catalysts for lithium-oxygen batteries. *Scientific reports* 6, 1-8 (2016). <https://doi.10.1038/srep24314>
- [44] S. Mickevičius, S. Grebinskij, V. Bondarenka, B. Vengalis, K. Šliužienė, B.A. Orłowski BA, V. Osinniy, W. Drube, Investigation of epitaxial LaNiO_{3-x} thin films by high-energy XPS.

Journal of alloys and compounds 423, 107-111 (2006). <https://doi.org/10.1016/j.jallcom.2005.12.038>

[45] T.L. Barr, Modern ESCA: The principles and practice of X-ray photoelectron spectroscopy. CRC press, 2020. <https://doi.org/10.1201/9781003069041>

[46] Y. Qiu, R. Gao, W. Yang, L. Huang, Q. Mao, J. Yang, L. Sun, Z. Hu, X. Liu, Understanding the Enhancement Mechanism of A-Site-Deficient La_xNiO_3 as an Oxygen Redox Catalyst. Chemistry of Materials 32, 1864-1875 (2020). <https://doi.org/10.1021/acs.chemmater.9b04287>

[47] C. Solís, L. Navarrete, J.M. Serra, Study of Pr and Co doped $\text{La}_2\text{NiO}_{4+\delta}$ as cathodes for $\text{La}_{5.5}\text{WO}_{11.25-\delta}$ based protonic conducting fuel cells. Journal of power sources 240, 691-697 (2013). <https://doi.org/10.1016/j.jpowsour.2013.05.055>

[48] B.C. Steele, Appraisal of $\text{Ce}_{1-y}\text{Gd}_y\text{O}_{2-y/2}$ electrolytes for IT-SOFC operation at 500 ° C. Solid state ionics 129, 95-110 (2000). [https://doi.org/10.1016/S0167-2738\(99\)00319-7](https://doi.org/10.1016/S0167-2738(99)00319-7)

[49] J.M. Porras-Vázquez, L. Dos Santos-Gómez, I. Santacruz, M.A. Aranda, D. Marrero-López, E.R. Losilla, Single step reactive sintering and chemical compatibility between $\text{La}_9\text{Sr}_1\text{Si}_6\text{O}_{26.5}$ and selected cathode materials. Ceramics International 38, 3327-3335(2012). <https://doi.org/10.1016/j.ceramint.2011.12.042>

[50] I.D. Raistrick, J.R. Macdonald, D.R. Franceschetti, Impedance spectroscopy. Emphasizing Solid Materials and Systems 27, (1987).

[51] E.J.L. Schouler, M. Kleitz, Electrocatalysis and inductive effects at the gas, Pt/stabilized zirconia interface. Journal of The Electrochemical Society 134, 1045 (1987). <https://doi.org/10.1149/1.2100614>

[52] L. Mogni, N. Grunbaum, F. Prado, A. Caneiro, Oxygen reduction reaction on Ruddlesden–Popper phases studied by impedance spectroscopy. Journal of The Electrochemical Society 158, B202-B207(2011). <https://doi.org/10.1149/1.3511770>

[53] S. Pang, X. Jiang, X. Li, Q. Wang, Z. Su, Characterization of Ba-deficient $\text{PrBa}_{1-x}\text{Co}_2\text{O}_{5+\delta}$ as cathode material for intermediate temperature solid oxide fuel cells. Journal of Power Sources 204,53-59 (2012). <https://doi.org/10.1016/j.jpowsour.2012.01.034>

[54] C.N. Ni, D.F. Zhang, C.Y. Ni, Z.M. Wang, Ruddlesden–Popper nickelate as coating for chromium-forming stainless steel. International Journal of Hydrogen Energy 39, 13314-13319 (2014). <https://doi.org/10.1016/j.ijhydene.2014.06.147>

[55] S.J. Kim, K.J. Kim, A.M. Dayaghi, G.M. Choi, Polarization and stability of $\text{La}_2\text{NiO}_{4+\delta}$ in comparison with $\text{La}_{0.6}\text{Sr}_{0.4}\text{Co}_{0.2}\text{Fe}_{0.8}\text{O}_{3-\delta}$ as air electrode of solid oxide the electrolysis cell. International Journal of Hydrogen Energy 41, 14498–14506 (2016). <https://doi.org/10.1016/j.ijhydene.2016.05.284>

- [56] D. Chen, R. Ran, K. Zhang, J. Wang, Z. Shao, Intermediate-temperature electrochemical performance of a polycrystalline $\text{PrBaCo}_2\text{O}_{5+\delta}$ cathode on samarium doped ceria electrolyte. *Journal of Power Sources* 188, 96-105 (2009). <https://doi.org/10.1016/j.jpowsour.2008.11.045>
- [57] W. Zhou, R. Ran, Z. Shao, W. Jin, N. Xu, Evaluation of A-site cation deficient $(\text{Ba}_{0.5}\text{Sr}_{0.5})_{1-x}\text{Co}_{0.8}\text{Fe}_{0.2}\text{O}_{3-\delta}$ ($x > 0$) perovskite as a solid-oxide fuel cell cathode. *Journal of Power Sources* 182, 24-31 (2008). <https://doi.org/10.1016/j.jpowsour.2008.04.012>
- [58] H. Zhao, F. Mauvy, C. Lalanne, J.M. Bassat, S. Fourcade, J.C. Genier, New cathode materials for ITSOFC: phase stability, oxygen exchange and cathode properties of $\text{La}_{2-x}\text{NiO}_{4+\delta}$. *Solid State Ionics* 179, 2000-2005 (2008). <https://doi.org/10.1016/j.ssi.2008.06.019>
- [59] M. Rieu, Preparation by sol-gel route and characterization of a complete SOFC cell on a porous metal support, Material Sciences Doctoral School, Interuniversity Center for Materials Research and Engineering - Cirimat, Carnot Institute, Ph.D thesis, (2009).
- [60] Y. Tao, Y. Zhou, W. Li, J. Shao, L. Bai, X. Liu, Intermediate-temperature solid oxide fuel cells with high performance cobalt-doped $\text{Pr}_{0.5}\text{Ba}_{0.5}\text{FeO}_{3-\delta}$ anodes. *Journal of Alloys and Compounds* 741, 1091-1097 (2018). <https://doi.org/10.1016/j.jallcom.2018.01.167>
- [61] L. Bian, L. Wang, C. Duan, C. Cai, X. Song, S. An, Co-free $\text{La}_{0.6}\text{Sr}_{0.4}\text{Fe}_{0.9}\text{Nb}_{0.1}\text{O}_{3-\delta}$ symmetric electrode for hydrogen and carbon monoxide solid oxide fuel cell. *International Journal of Hydrogen Energy* 44, 32210-32218 (2019). <https://doi.org/10.1016/j.ijhydene.2019.10.090>